The late Cenozoic channel migration of the Yangtze River in the delta region: insights from cosmogenic nuclide burial dating on the onshore boreholes

Yu Liu[1, 2], Xianbin Liu[3], Shijie Wang[1, 2], Sheng Xu[4], Rob Ellam[4, 5], Derek Fabel[5], Jing Chen[6*]

[1] State Key Laboratory of Environmental Geochemistry, Institute of Geochemistry, Chinese Academy of Sciences, Guiyang 550081, China

[2] Puding Karst Ecosystem Research Station, Chinese Academy of Sciences, Puding 562100, China

[3] School of Resource and Environmental Engineering, Ludong University, Yantai 264025, China

[4] Institute of Surface-Earth System Science, School of Earth System Science, Tianjin University, Tianjin 300072, China

[5] Scottish Universities Environmental Research Centre, East Kilbride, G75 0QF, United Kingdom

[6] State Key Laboratory of Estuarine and Coastal Research, East China Normal University, Shanghai 200062, China

[*] Corresponding author: jchen@geo.ecnu.edu.cn (Jing Chen)

Abstract:

A thorough magnetostratigraphic chronology of the Yangtze delta is problematic due to coarse-grained (i.e. poorly magnetized) deposits and sedimentary discontinuity. This study presents cosmogenic nuclide data that facilitate $^{26}Al/^{10}Be$ burial dating which is used to determine the absolute age of the important provenance change layer (from

local to the Yangtze River) in four onshore boreholes in the delta region which provide an independent check on previous paleomagnetic results. Sediments near the provenance change beds of boreholes RGK15 and ZKJ39 in the northern delta yielded ages of 4.99 (+1.26/-0.81) Ma and 4.74 (+0.94/-0.70) Ma, which are the oldest radiometric ages yet from the many boreholes in the delta. The sediments of the provenance shift layer in two boreholes LQ19 and LQ11 from the southern delta produced burial ages of 0.94 (+0.17/-0.16) Ma and 0.57 ± 0.17 Ma, respectively. Combining these ages with previous lithofacies and provenance studies indicate that the modern Yangtze River first flowed through the northern delta prior to ~5 Ma, then migrated southward to the present estuary location after 0.94 Ma and the mainstream channel, or a branch thereof, moved further south at 0.57 Ma. The southward migration history of the Yangtze channel is possibly a response to tectonic subsidence of the Zhe-Min Uplift during the middle Quaternary. Our results constrain the emergence of the modern Yangtze River in the delta area before ~5 Ma, and provide a new chronology for further study of the evolution of the Yangtze River drainage basin.

Key words:

$^{26}Al/^{10}Be$, burial age, borehole, channel migration, Yangtze delta

1. Introduction

As a result of the India-Eurasia collision starting in the early Cenozoic, uplift of the Tibetan Plateau has not only changed crustal deformation and atmospheric

circulation patterns (e.g. Molnar and Tapponnier, 1975; Molnar et al., 1993; Chuang et al., 1998; An et al., 2001; Tapponnier et al., 2001; Wang et al., 2008), but also changed the regional topographical gradient, with eastern Asia reversing its regional tilt from westward to eastward (Wang, 2004). Reversal of the continental gradient may have triggered reorganization of major river systems (Brookfield, 1998; Clark et al., 2004). Originating on the eastern Tibetan Plateau and flowing into the East China Sea, the Yangtze River is one of the world's longest rivers. The Cenozoic imposed dramatic changes of the macroscopic geomorphology of China are recorded in the evolution of the Yangtze River, which has been extensively studied for more than a century, but have implications that remain controversial.

The first evolutionary model of the Yangtze River was proposed by Barbour (1936) with refinements incorporated by Clark et al. (2004) is now broadly accepted. Much of the outstanding debate surrounding this model relates to the timing of a series of river capture events in the Cenozoic. Two regions are mainly focused: First Bend and Three Gorges (Fig. 1a). First Bend (FB) is located at the northwestern Yunnan Plateau (Fig. 1a), where tectonic structures have been related to the timing diversion of the Yangtze River away from the Red River flowing into the South China Sea (Clark et al., 2004; Clift et al., 2008b; Kong et al., 2012; McPhillips et al., 2016). Three Gorges (TG) is at eastern margin of the Sichuan Basin (SCB; Fig. 1a), where the previously southwest flowing Chuan Jiang (a segment of the Yangtze River in the Sichuan Basin) was progressively captured by the eastward draining mid-lower Yangtze River (Li et al., 2001; Xiang et al., 2007; Zhang et al., 2008; Richardson et al., 2010; Wang et al., 2014;

Shao et al., 2012, 2015). Currently, there is no consensus on the formation of the Yangtze River and there is a particularly large uncertainty about the timing of connection of the Three Gorges with estimates ranging from 0.12 to 45 Ma (see Fig. 2 of Gu et al., 2014).

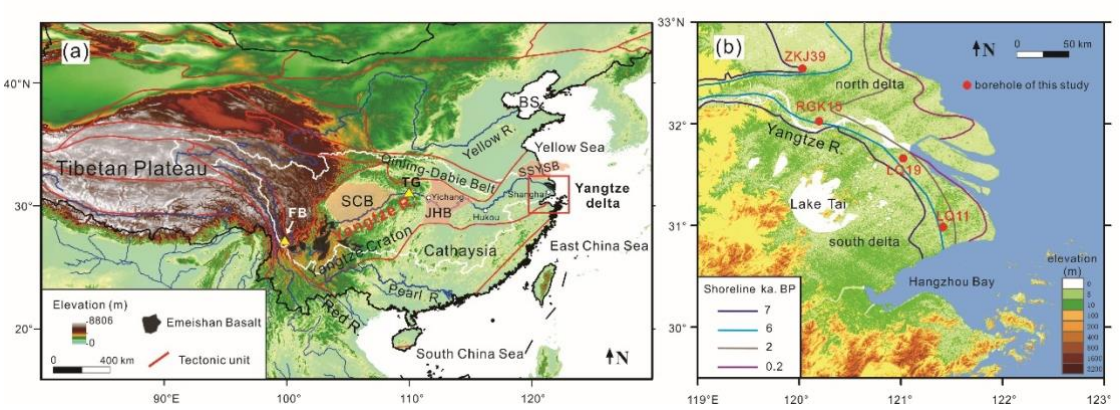

Figure 1. (a) Geomorphologic map of East Asia showing the Yangtze drainage basin (white line) and location of the Yangtze delta in the red box. BS: Bohai Sea; SSYSB: Subei-South Yellow Sea Basin; SCB: Sichuan Basin; JHB: Jianghan Basin; FB: First Bend; TG: Three Gorges. (b) Schematic map of four studied borehole locations (red dots) in the modern Yangtze delta. The position and age of the old shorelines are after Saito et al (2001).

Based on "source to sink" theory, various provenance approaches have been performed in the Yangtze delta, whose sedimentary record is a significant repository of drainage information, providing potential insights into the Yangtze River evolution. Previous studies traced the provenance of the Yangtze River through the late Cenozoic, using sediment provenance proxies such as heavy minerals, clay mineral, geochemistry, magnetism and zircon geochronology (Fan et al., 2005; Yang et al., 2006; Chen et al., 2009; Gu et al., 2014; Zheng et al., 2013; Liu et al., 2018; Yue et al., 2019; Yu et al., 2020). One consensus has been reached that a major provenance shift related to the Yangtze River occurred earlier in the north delta than in the south delta during Pliocene to Early Pleistocene based on the paleomagnetic chronology (Liu et al., 2018; Yue et al., 2019; Yu et al. 2020).

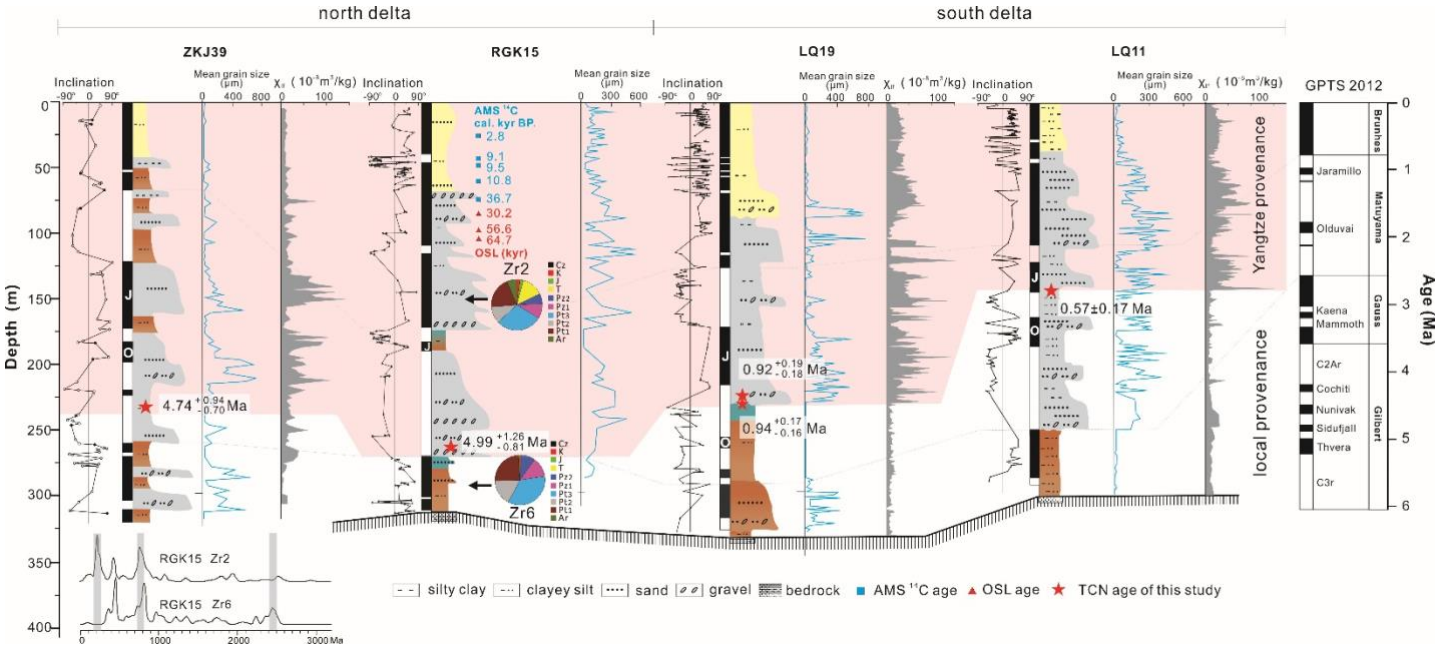

Figure 2. Lithology, magnetostratigraphy, mean grain size, magnetic susceptibility (χ_{lf}) and absolute age of studied boreholes in the modern Yangtze delta. The geomagnetic polarity timescale (GPTS) is from Cande and Kent (1995). Pink shading marks higher magnetic susceptibility in the upper cores and indicates Yangtze River-derived provenance. Normalized relative age probability diagrams of detrital zircons from depth 150 m (Zr2) and 290 m (Zr6) of core RGK15 and their proportions are shown in pie charts. Data of the detrital zircon, ^{14}C age and OSL age of core RGK15 are all sourced from Yu et al. (2020).

Paleomagnetic dating provides relative chronology by comparison of polarity reversals recorded in local cores with the well-established global standard sequence. A successful paleomagnetic chronology depends on the continuity of the stratigraphic sequence in the local cores. However, coarse fluvial deposits frequently occur in the Plio-Pleistocene stratigraphy of the Yangtze delta, implying erosive activity and consequent stratigraphic discontinuity which will deleteriously affect sampling continuity and hence paleomagnetic data integrity (see inclination and polarity in Fig. 2). Thus, some important boundary or polarity events used to assemble a chronological model for the major provenance shift are ambiguous and potentially unreliable. Key stratigraphic markers related timing the shift in the north and the south delta that are less than definitive include the Gauss - Matuyama reversal and the Jaramillo subchron

(Chen et al., 2009; Gu et al., 2014; Liu et al., 2018; Yue et al., 2019; Yu et al. 2020). This is a common problem with chronology of the late Cenozoic deposition in the delta region, and limits our understanding on the geomorphological evolution of the Yangtze River and its delta (Fan et al., 2004; Yang et al., 2006; Chen et al., 2009; Gu et al., 2014; Liu et al., 2018; Yue et al., 2019; Yu et al. 2020).

Coarse deposits are non-ideal for magnetostratigraphy but are the preferable medium for *in-situ* terrestrial cosmogenic nuclide (TCN) radiometric dating. TCN-dating has become increasingly reliable as a method for dating geomorphic surfaces and measuring process rates over 10^2-10^6 year time scales (Balco et al., 2008; Kong et al., 2012; Liu et al., 2013; Granger, 2014; McPhillips et al., 2016; Blard et al., 2019). In view of the importance of the site and its stratigraphy, an attempt to date provenance shift layers from four onshore boreholes in the Yangtze delta was performed by cosmogenic ^{26}Al-^{10}Be burial dating. We aim to provide an independent check on the results of previous magnetostratigraphy. In particular, we try to assess the radiometric ages of these provenance shift sediments to provide insights into Yangtze channel migration history in the estuarine region as well as indicative for the evolution of the Yangtze drainage basin.

2. Geological setting

The Yangtze River with a length of ~6300 km, drains eastward through three major topographic steps within China and discharges into the East China Sea (Figure 1a). The Yangtze basin covers a vast area (~1.8×10^6 km^2), with substantial topographical contrast reflecting complex geology (Figure 1a). The Yangtze water course may be

128 divided into (upper) the section from the headwaters to the east end of the Three Gorges
129 (Yichang city), (middle) from Yichang city to Hukou city (estuary of the Lake Poyang)
130 and (lower) from Hukou city to the East China Sea. The middle and lower Yangtze
131 sections are approximately 1200 km in length, and along the full length of the river
132 mean altitude of drainage decreases abruptly from 2000 m to under 500 m. Changing
133 topography is reflected by flow velocity which is quickly reduced to develop a
134 meandering river. Three large basins are mainly distributed in the three reaches, the
135 upstream Sichuan Basin (SCB) in the west is connected to the middle Jianghan Basin
136 (JHB) by the Three Gorges, which is in turn connected to the lower Subei-South Yellow
137 Sea Basin (SSYSB) to the north of the modern Yangtze delta. Apart from a few hundred
138 meters of Quaternary sediments deposited in the west Chengdu plain, the SCB was
139 characterized by widespread erosion during the Cenozoic (Richardson et al., 2008). In
140 contrast, thick fluvial and lacustrine sediments were deposited in the downstream JHB
141 (Wang et al., 2014) and SSYSB basins (Qiang et al., 1997).

142 Geologically, the Yangtze drainage basin comprises several tectonic systems.
143 From west to east, these include the Qamdo Block, the Songpan-Garze terrane, the
144 Qinling-Dabie orogenic belts, the Yangtze Craton and the Cathaysia Block (Figure 1a).
145 The upper reaches are dominated by Paleozoic-Mesozoic carbonate and clastic rocks,
146 with a large-scale Mesozoic basaltic outcrop (the Emeishan Basalt; Fig 1a) and some
147 Cenozoic felsic igneous rocks (Changjiang Water Resources Commission, 1999).
148 Previously, the Emeishan Basalt, which has characteristic geochemistry and magnetic
149 properties (high χlf, SIRM and S-ratio, and low χARM/χlf and χARM/SIRM), has been

widely used as a key tracer of the upper reach provenance in the downstream basins, and is indicative of connection of the Three Gorges (e.g. Zhang et al., 2008; Chen et al., 2009; Gu et al., 2014; Shao et al., 2015; Liu et al., 2018). The middle and lower reaches are primarily dominated by Paleozoic-Mesozoic sedimentary rocks and unconsolidated Quaternary sediments, with some felsic igneous rocks and metamorphic rocks (Changjiang Water Resources Commission, 1999).

The Yangtze delta (30°20'-32°30' N，119°24'-122°30' E) lies east of the Yangtze Block where the channel is no longer controlled by bedrock, is the most downstream terrestrial depocenter before the Yangtze River flows into the sea. The Yangtze delta depression was formed due to the extension by Pacific-Eurasia convergence during Paleocene (Ren et al., 2002). The modern delta plain was formed by 1.7×10^{12} tons of sediments transported by the Yangtze River over the past 7 ka as sea level evolved towards its present position (Figure 1b; Saito et al., 2001). The Yangtze delta is composed of the north and south delta plains divided by the main channel (Fig. 1b). The terrain of delta plain is low and flat with an average altitude of ~4 m. Except for a few bedrock monadnock in the southern plain, most area is covered by loose late Cenozoic sediments that deposited unconformably on bedrock with a thickness of >1000 m in the north and 200-400 m in the south delta (Chen and Stanley, 1995).

3. Material and Methods

3.1 Borehole description and sampling

Core ZKJ39 (32°30'11"N, 120°02'05"E) with a length of 322.2 m drilled into the north Yangtze delta (Figure 1b) did not reach bedrock. Lithology, sedimentary facies,

heavy minerals, zircon morphological character, magnetostratigraphy, magnetic properties and foraminifera were recorded and are described in Yue et al. (2016) and Liu (2018) (Figure 2). These previous studies indicate that a significant provenance shift occurred at depth of 235 m with the upper sediments derived from the Yangtze River. A sand sub-sample at depth of 231.5 m was collected from this core for ^{26}Al-^{10}Be burial dating.

Core RGK15 (32°7'1"N, 120°28'59"E) with a length of 318 m down to the Cretaceous bedrock was recovered by rotary drilling from the vertex of the north Yangtze delta plain (Figure 1b). Detailed lithology, sedimentary facies and chronology determined by paleomagnetic, optically stimulated luminescence (OSL) and AMS ^{14}C methods were described in Yu et al. (2020) (Figure 2). Heavy minerals and zircon U-Pb ages reveal a significant provenance shift at a depth of 272 m, which is ~2.6 Ma according to the paleomagnetic chronology (Yu et al., 2020). A sand layer at depth of 269 m, was collected for ^{26}Al-^{10}Be burial dating.

Core LQ19 (31°28'22"N, 121°19'44"E) was drilled in northwest Shanghai city, to the west of the present Yangtze channel (Figure 1b). The core was continuously drilled to a depth of 330.9 m and reached Cretaceous bedrock. Lithology, sedimentary facies, magnetostratigraphy, magnetic properties and foraminifera were recorded and described in Liu (2018) (Figure 2). Many magnetic parameters show an abrupt change at a depth of 225 m suggesting that the sediment beneath this depth was of local provenance and sediment above 225 m was dominated by Yangtze River deposition. Two sand samples from depth of 225 m and 223 m were collected respectively for ^{26}Al-

^{10}Be burial dating.

Core LQ11 (31°01'43"N, 121°22'7"E) with a continuous 301 m length to the Jurassic bedrock was recovered by rotary drilling from the southern Yangtze delta plain in Shanghai city (Figure 1b). Sedimentary facies, lithology, magnetic properties, magnetostratigraphy, organic carbon analysis and foraminifera identification were recorded for this core, and are described in detail by Liu et al. (2018). Magnetic properties characterized by high χ_{lf}, SIRM, S_{-300} and low χ_{ARM}/SIRM suggest a profound sediment provenance change at a depth of 145 m with an inferred palaeomagnetic age of 1.0-1.2 Ma (Liu et al., 2018). A sand layer at depth 145 m was sub-sampled for ^{26}Al-^{10}Be burial dating.

3.2 Sample preparation and analysis

The five coarse sand samples from four boreholes were sieved to 0.25-0.5 mm. Quartz was separated and purified in the State Key Laboratory of Environmental Geochemistry (SKLEG), Institute of Geochemistry, Chinese Academy of Sciences. Beryllium and aluminum extraction and purification, accelerator mass spectrometry (AMS) measurement of ^{26}Al and ^{10}Be concentration, and total Al determination by inductively coupled plasma optical emission spectrometry (ThermoFisher Scientific iCAP 7400, assigned 3% uncertainty) were all performed at the Scottish Universities Environmental Research Centre (SUERC). The 0.125-0.25 mm size fraction was used for quartz purification by selective chemical dissolution (Kohl and Nishiizumi, 1992). The purified quartz (10-20 g) was dissolved in a solution of concentrated HF and HNO_3. Approximately 0.2 mg Be carrier was added to the samples and a procedural blank. Al

carrier (1.0 mg) was added only to the blank. The Al and Be were extracted and separated by ion chromatography and selectively precipitated as hydroxides. The precipitates were oxidized at 800°C. The Al_2O_3 and BeO were mixed with Ag and Nb matrix respectively with weight ratios of Al_2O_3:Ag=1:2 and BeO:Nb=1:6 for AMS analysis (Xu et al., 2015). The procedural blank processed in association with the samples has a $^{10}Be/^{9}Be$ of $(5.63 \pm 0.66) \times 10^{-15}$ and $^{26}Al/^{27}Al$ of $(1.12 \pm 0.79) \times 10^{-15}$. Measured $^{26}Al/^{27}Al$ and $^{10}Be/^{9}Be$ ratios are normalized to primary standards Z92-0222 with a nominal $^{26}Al/^{27}Al$ ratio of 4.11×10^{-11} and NIST SRM 4325 with a nominal $^{10}Be/^{9}Be$ ratio of 2.79×10^{-11}, respectively.

3.3 $^{26}Al/^{10}Be$ simple burial dating

Cosmogenic nuclide burial dating uses measurements of the concentration of cosmic ray produced terrestrial ^{10}Be and ^{26}Al in samples that were exposed at Earth's surface prior to deposition and subsequent shielding from cosmic rays. Once buried, the ^{26}Al and ^{10}Be concentrations decrease due to radioactive decay, and the faster decay of ^{26}Al results in a decrease in the $^{26}Al/^{10}Be$. The $^{26}Al/^{10}Be$ ratio is used to derive a burial age assuming closed system behavior (Granger and Muzikar 2001; Granger, 2006; Granger, 2014).

The long-term concentration (N_i) of ^{26}Al or ^{10}Be in quartz that is exposed near the surface and then buried follows the relationship:

$$N_i = N_{i,inh} e^{(-t/\tau_i)} + N_{i,pb} \quad (1)$$

where subscript *i* represents either ^{26}Al or ^{10}Be, *inh* indicates inheritance prior to burial, t is burial age, τ is the radioactive mean life and *pb* indicates the total post-burial

production. In a landscape that is eroding steadily at a rate E, the inherited nuclide concentration is:

$$N_{i,inh} = P_n / (1/\tau_i + \rho E/\Lambda_n) + P_\mu / (1/\tau_i + \rho E/\Lambda_\mu) \quad (2)$$

where P_n, P_μ and Λ_n, Λ_μ are the production rates (atoms/g/yr) and penetration lengths (g/cm^2) due to neutrons and muons (negative muon and fast muon), respectively. ρ indicates rock density. Simple burial dating assumes that the sample was exposed at the surface with a high concentration of inherited nuclides and was then buried deeply enough (typically more than 10 m) that post-burial production can safely be ignored. In this case, Eq. (1) simplifies to

$$N_{26}/N_{10} = (N_{26,inh}/N_{10,inh}) e^{-t(1/\tau_{26} - 1/\tau_{10})} \quad (3)$$

Eq. (2) and Eq. (3) can be solved iteratively for converging solution of burial age t and pre-burial erosion rate E.

The basic premise of burial dating is that sediment is buried deep enough to avoid significant post-burial nuclide production and has a simple exposure history prior to burial. Thus, simple burial dating is ideal for dating cave sediments or very thick fluvial deposits. However, complex exposure-burial histories cannot be ruled out, making all burial ages maximum ages. The current burial dating method limits range roughly between 0.1 and 5 Ma (Granger, 2014).

Our sampled boreholes are located at the river-mouth of the Yangtze River, its upstream area is large and landscape is complicated (Figure 1a). Therefore, the average latitude (30°N) and average altitude of drainage basin (2000 m) were considered to calculate the production rates. Cosmogenic nuclide production rates were assumed

constant for the basin and were calculated as P_{10}=15.0 atoms/g/yr and P_{26}=101.7 atoms/g/yr including neutron and muon contributions. Cosmogenic nuclide production rates and burial ages were calculated using CRONUS-earth online calculator v.2.3 MATLAB code (Balco et al., 2008). For an assumed rock and overlying sediment density of 2.60 g/cm^3, the exponential penetration length for any nucleon is 160 g/cm^2 (Masarik and Reedy, 1995), whereas negative muon and fast muon penetration lengths are 1510 g/cm^2 and 4320 g/cm^2, respectively (Heisinger et al., 2002a, b). The radioactive mean lives of ^{26}Al (τ_{26}=1.021 ± 0.024 Ma; Nishiizumi, 2004) and ^{10}Be (τ_{10}=2.005 ± 0.017 Ma; Chmeleff et al., 2010) were used. Burial age calculation assumes a rapid deposition rate and no cosmogenic nuclide post-production.

4. Results and Discussion

All analytical results are listed in Table 1 and shown in Figure 3. The stated errors are 1σ calculated from AMS and ICP-OES uncertainties. Samples RGK15 and ZKJ39 in the north delta have very low measured ^{26}Al/^{27}Al ratios of 0.29 ± 0.11 × 10^{-14} and 0.40 ± 0.12 × 10^{-14}, respectively. The procedural blank represents 38% and 28 % of the ^{26}Al atoms, respectively. Compared with Al, ^{10}Be/^{9}Be ratios of these two samples are four times higher than the blank. Low concentrations of both ^{26}Al and ^{10}Be in samples RGK15 and ZKJ39 result in low ^{26}Al/^{10}Be ratios with large uncertainties. This effect is most extreme for sample RGK15 with approximately 50% uncertainty and results in the oldest burial age of 4.99 (+1.26/-0.81) Ma. Improved data precision could be achieved by using larger amounts of quartz to increase AMS counting statistics. However, the amount of borehole samples is limited and only a small yield of coarse

sand remained after sieving and purification. A similar situation also occurred in the southern delta borehole (LQ19) for which each sample gave only ~10 g of quartz. Therefore, 4.99 (+1.26/-0.81) Ma and 4.74 (+0.94/-0.70) Ma with relatively large uncertainties were the best results obtainable from boreholes RGK15 and ZKJ39 respectively. For the southern delta cores, LQ11 has a burial age of 0.57 ± 0.17 Ma while the burial age of core LQ19 at depth of 223 m is 0.92 (+0.19/-0.18) Ma, which is in a good agreement with burial age 0.94 (+0.17/-0.16) Ma of sediment at depth 225 m.

Table 1. Cosmogenic ^{26}Al and ^{10}Be results of the studied boreholes from the Yangtze delta

Borehole	Sample depth (m)	Quartz mass (g)	^{27}Al in quartz (ppm)	$^{26}Al/^{27}Al$ (10^{-14})	$^{10}Be/^{9}Be$ (10^{-14})	Concentration (atoms/g)		$^{26}Al/^{10}Be$	Model burial age (Ma)
						^{26}Al (10^4)	^{10}Be (10^4)		
LQ11	145	14.98	125±6	15.04±0.82	8.63±0.26	41.81±3.10	8.04±0.28	5.20±0.43	0.57±0.17
LQ19	223	10.04	137±7	10.01±0.59	5.22±0.20	30.41±2.38	6.91±0.32	4.40±0.40	0.92 (+0.19/-0.18)
	225	10.86	114±6	17.10±0.79	7.79±0.27	43.12±2.95	9.91±0.40	4.35±0.35	0.94 (+0.17/-0.16)
RGK15	269	20.98	138±7	0.29±0.11	2.31±0.15	0.76±0.35	1.23±0.12	0.62±0.29	4.99 (+1.26/-0.81)
ZKJ39	231.5	20.17	123±6	0.40±0.12	2.47±0.26	0.98±0.35	1.40±0.20	0.70±0.27	4.74 (+0.94/-0.70)

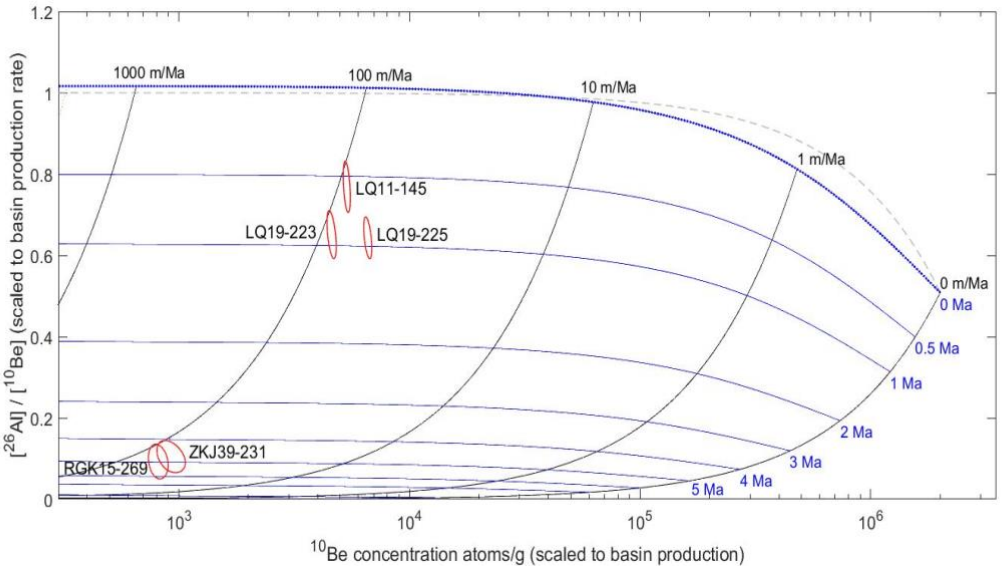

Figure 3. Cosmogenic nuclide data from studied boreholes in the Yangtze delta, shown on a logarithmic graph of $^{26}Al/^{10}Be$ versus ^{10}Be concentration.

4.1 Comparison of cosmogenic nuclide burial age and magnetostratigraphy in the Yangtze delta

The magnetostratigraphy of the four studied cores in the Yangtze delta (Figure 2) are derived from Liu et al. (2018), Yu et al. (2020), and Liu (2020). Paleomagnetic analysis of core LQ11 reveals the Gauss normal chron at a depth between 300 m and 252 m, and the Matuyama reversed chron between 252 and 112 m. The Olduvai and Jaramillo subchrons are recognized at depths of 186-160 m and 145-121 m, respectively. The Brunhes normal chron is evident above 112 m. Therefore, the paleomagnetic age of the significant provenance shift to Yangtze-derived sediments at depth of 145 m is near the base of the Jaramillo subchron at ~1.0-1.2 Ma (Liu et al., 2018). This age is nearly double the $^{26}Al/^{10}Be$ burial age of 0.57 ± 0.17 Ma.

Similarly, three chrons including Gauss, Matuyama and Brunhes were also recognized in other borehole sediments of LQ19, ZKJ 39 and RGK 15 (Figure 2). For core LQ19, the Olduvai and Jaramillo subchrons are inferred at depths of 260-254 m and 155-148 m, respectively. This means that the provenance shift sediment at a depth of 225 m should be between 1.05 and 1.78 Ma, most likely around 1.0-1.2 Ma (Liu et al., 2018). This is the only paleomagnetic age that is coincident with the cosmogenic burial age of 0.94 (+0.17/-0.16) Ma within uncertainty. The $^{26}Al/^{10}Be$ burial age at depth of 223 m, 2 m shallower sand yields a similar age of 0.92 (+0.19/-0.18) Ma, suggesting rapid fluvial deposition.

For core ZKJ39, correlation of the magnetic polarity sequence to the geomagnetic polarity timescale suggested that the Olduvai and Jaramillo subchrons are inferred at depths of 199-168 m and 151-122 m, respectively (Figure 2; Liu et al., 2018). Hence, the paleomagnetic age of the provenance shift sediment at depth of 234.5 m should be

316 older than the Olduvai subchron and younger than the Gauss chron (1.9-2.6 Ma). Our
317 dated sand at depth of 231.5 m that is 3 meters shallower yields a burial age of 4.74
318 (+0.94/-0.70) Ma, indicating that the provenance shift event in core ZKJ39 should have
319 occurred earlier than this age. For core RGK15, the Pliocene/Pleistocene boundary
320 occurs at 272 m and the Early/Middle Pleistocene boundary is located at 173 m (~0.78
321 Ma; Figure 2; Yu et al., 2020). Therefore, the paleomagnetic age of provenance shift
322 sediment at depth of 272 m should be around 2.60 Ma. However, the cosmogenic
323 $^{26}Al/^{10}Be$ ratio at depth 269 m yields a burial age of 4.99 (+1.26/-0.81) Ma. These two
324 old radiometric ages are consistent with new detrital zircon U-Pb ages from the East
325 China Sea Shelf Basin that suggest the present-day Yangtze River was established in
326 the late Miocene (Fu et al., 2021). Thus, the absolute age constrained by cosmogenic
327 $^{26}Al/^{10}Be$ indicates that the paleomagnetic ages of cores ZKJ39 and RGK15 may have
328 been significantly underestimated in previous studies.

329 Apparently, the magnetostratigraphy of the four studied cores in the Yangtze delta
330 are only occasionally in accordance with cosmogenic nuclide absolute ages, and may
331 overestimate or underestimate the sediment deposition age. The discrepancies most
332 likely reflect the complexity of river and ocean sedimentary systems, particularly
333 during the Quaternary. Sediment and mineral compositions vary in estuarine
334 environments, and/or river channel migration resulted in discontinuous sedimentation
335 and variable deposition rates (Morton, 1984; Chen and Stanley, 1995). Together with
336 coarser fluvial sediments (e.g. sand and pebble) that repeatedly appear in the deposition
337 sequence, especially for the Pliocene and early Pleistocene sediments (Figure 2), these

factors may have significantly affected the precision of paleomagnetic ages.

4.2 Yangtze River channel migration in the delta region during the late Cenozoic

The cosmogenic $^{26}Al/^{10}Be$ burial ages and previous provenance study of four cores generally show a channel migration history of the Yangtze River in the delta region during the late Cenozoic (Figure 4). Before the modern Yangtze River flowed through the location of core ZKJ39 and RGK15, the sediments were mainly sourced from the local bedrock or adjacent mountains that characterized by low ferrimagnetic content, simple heavy minerals and zircon age spectrum which are quite different from that of the modern Yangtze River (see Figure 3 and 5 in Yu et al. (2020); Figure 2; Wang et al., 2006; Yue et al., 2019). When the modern Yangtze River arrived, the sediments ferrimagnetic content remarkably increased and the magnetic grain size got coarser in core ZKJ39, and heavy minerals diversified, multiple peaks of the zircon age spectrum and the occurrence of Mesozoic and Cenozoic zircons in core RGK15 indicate that the provenance area has expanded to the Tibetan Plateau and is similar with those of the modern Yangtze River. Combined with burial ages close to the provenance shift layers of cores ZKJ39 and RGK15 suggest that the modern Yangtze River firstly flowed through the north delta before 4.74-4.99 Ma (Figure 2 and 4a).

Then the Yangtze channel migrated southward to the modern river mouth after 0.92-0.94 Ma, resulted in the sediments ferrimagnetic content abruptly increased at depth of 225 m in core LQ19. A similar abrupt increase of ferrimagnetic content are also observed in core LQ11 and suggest that the mainstream channel or possibly just one branch of the channel moved further south (where core LQ11 is at present) after 0.57 Ma (Figure 4b). The southward migration of the Yangtze River resulted in abandonment of original channel in the northern delta, may cause sedimentary hiatuses or the sediment deposition rate fast decrease. For core RGK15, the TCN age at depth

of 270 m reaches 4.99 Ma and then fast decreases to 64.7 ka at depth of ~110 m by OSL dating. For core ZKJ39, both the sediment ferrimagnetic content and grain size were decreased in the upper part (135-0 m). At present, the south Yangtze channel (core LQ11) is disappeared and develops to the current channel pattern (Figure 4c).

This migration history and age interpretation are supported by recent studies on core CSDP-1 in the western offshore area of the South Yellow Sea, which is approximately 300 km northeast of core ZKJ39. Magnetostratigraphy together with clay mineral assemblages and Sr-Nd isotopes indicate that sediment provenance was mainly dominated by the Yangtze River before ~0.8 Ma with a shift to the Yellow River afterwards (Figure 4b; Liu et al., 2014; Zhang et al., 2019). This conclusion suggests southward migration of the Yangtze delta after 0.8 Ma, which is consistent with the cosmogenic burial ages on the Yangtze River provenance shift layer of core LQ19 (~0.9 Ma).

The southward migration of the Yangtze River is likely to have been in response to accelerated tectonic subsidence of the eastern China coast and the Zhejiang-Fujian Uplift (Qin et al., 1989; Chen and Stanley, 1995; Li et al., 2011). The Zhejiang-Fujian Uplift (abbreviated as the Zhe-Min Uplift) extends from Zhejiang and Fujian Province of China's southeastern coast to the southern Korean Peninsula, and it was once a natural barrier that blocked the incursion of sea water from the East China Sea before the Quaternary (Jin and Yu, 1982). The Zhe-Min Uplift began to subside in the early Pleistocene and marine transgression gradually spread northward, with sea-land interaction first observed in boreholes of the South Yellow Sea no later than 1.7 Ma and eventual subsidence below sea level at ~ 0.2 Ma (Wageman et al., 1970; Liu et al.,

2014; Yi et al., 2014, 2016; Mei et al., 2016). Therefore, before the early Pliocene (~5 Ma), the Yangtze delta region was still elevated, especially the south area within the Zhe-Min Uplift, constraining the Yangtze River to only flow through the north delta region with relative low altitude and slope. With Quaternary subsidence of the Zhe-Min Uplift, and particularly accelerated subsidence around 0.8 Ma (Liu et al., 2014, 2016; Mei et al., 2016; Zhang et al., 2019), the Yangtze River channel began to migrate southward arriving at the modern river mouth after ~0.9 Ma.

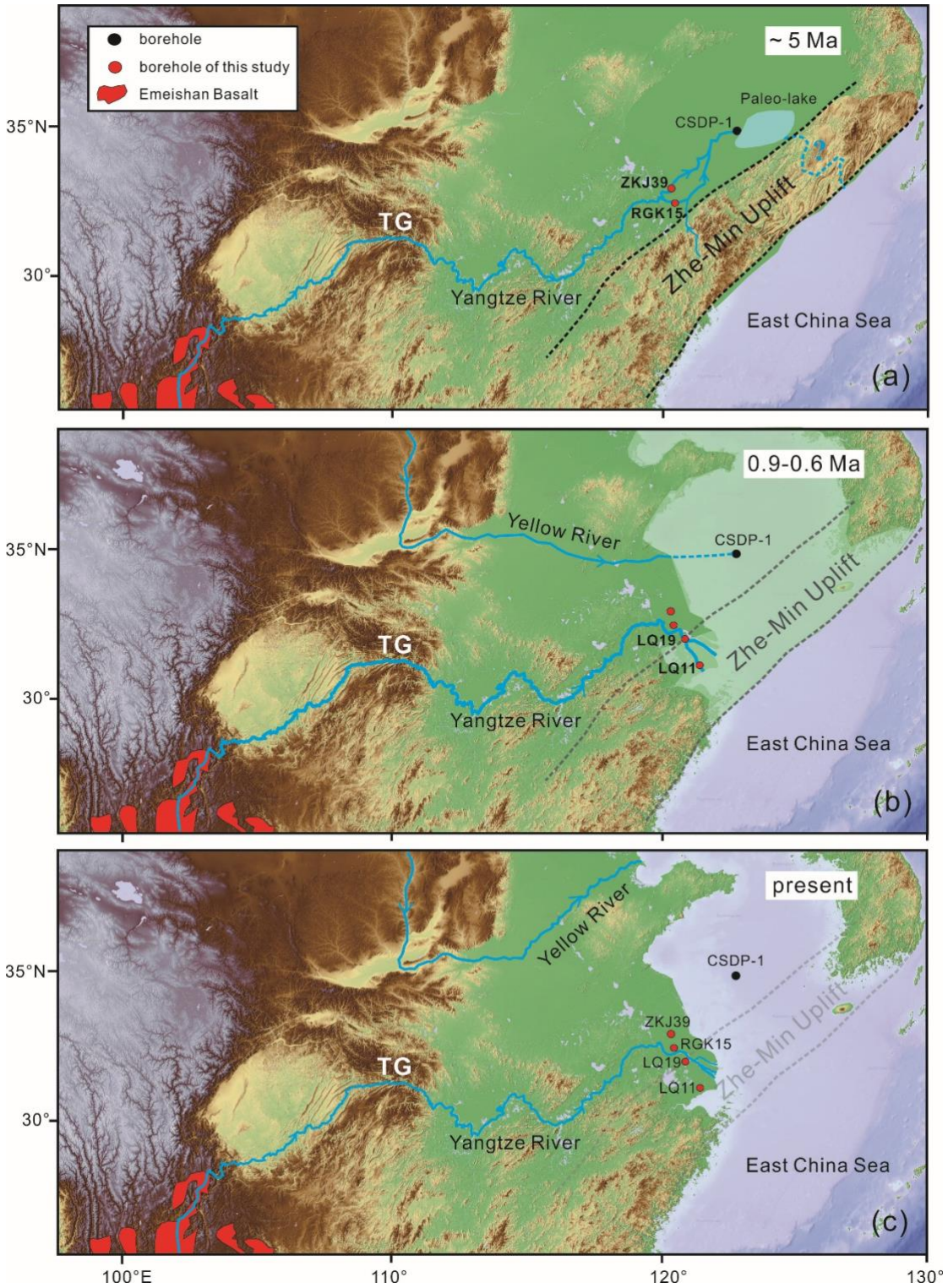

Figure 4. Time scales of schematic diagrams illustrate the southward migration of the Yangtze channel in the Yangtze delta area. (a) Before ~5 Ma, the Yangtze River flowed through the north delta area (location of core ZKJ39 and RGK15) into the South Yellow Sea paleo-lake due to the barrier of the Zhe-Min Uplift; (b) After ~0.9 Ma, the Yangtze River migrated southward and flowed into the East China Sea through the south delta area (location of core LQ19 and LQ11) due to the Zhe-Min Uplift subsidence; (c) At present, the Zhe-Min Uplift has subsided below sea level and a southern channel of the Yangtze River has disappeared (location of core LQ11).

5. Conclusion

The important provenance shift layer found in four onshore boreholes in the Yangtze delta has been dated for the first time by the cosmogenic $^{26}Al/^{10}Be$ burial method. Combined with previous lithofacies and provenance studies, sediments sourced from the modern Yangtze River in two cores RGK15 and ZKJ39 yield the burial ages of 4.99 (+1.26/-0.81) Ma and 4.74 (+0.94/-0.70) Ma respectively, indicating that the modern Yangtze River was initially depositing sediment in the north delta ~5 Ma ago. A provenance shift from a proximal source to the Yangtze River in two cores LQ19 and LQ11 from the southern delta yielded burial ages of 0.94 (+0.17/-0.16) Ma and 0.57 ± 0.17 Ma, respectively. Our study not only ahead the emergence of the modern Yangtze River in the delta area prior to ~5 Ma, but also suggests a southward migration of the Yangtze channel after ~0.9 Ma, which possibly resulted from the tectonic subsidence of the Zhe-Min Uplift during the middle Quaternary.

Acknowledgments

We thank María Miguens-Rodríguez for cosmogenic nuclide sample preparation. This research was funded by the Strategic Priority Research Program of the Chinese Academy of Sciences (XDB40020300) and the National Natural Science Foundation of China (grant number 41473055, 41771226, 41401009 and 41620104004).

Reference

An, Z.S., Kutzbach, J.E., Prell, W.L., Porter, S.C., 2001. Evolution of Asian monsoons and phased

421 uplift of the Himalaya-Tibetan plateau since late Miocene times. Nature. 411, 62-66.
422 Balco, G., Stone, J.O., Lifton, N.A., Dunai, T.J., 2008. A complete and easily accessible means of
423 calculating surface exposure ages or erosion rates from Be-10 and Al-26 measurements.
424 Quaternary Geochronology. 3, 174-195.
425 Barbour, G.B., 1936. Physiographic History of the Yangtze. Geographical Journal. 87, 17-34.
426 Blard, P.H., Lupker, M., Rousseau, M., 2019. Paired-cosmogenic nuclide paleoaltimetry. Earth and
427 Planetary Science Letters. 515, 271-282.
428 Brookfield, M.E., 1998. The evolution of the great river systems of southern Asia during the
429 Cenozoic India-Asia collision: rivers draining southwards. Geomorphology. 22, 285-312.
430 Cande, S.C., Kent, D.V., 1995. Revised calibration of the geomagnetic polarity timescale for the
431 Late Cretaceous and Cenozoic. Journal of Geophysical Research. 100, 6093-6095.
432 Changjiang Water Resources Commission, 1999. Atlas of the Changjiang River Basin. Chinese
433 Atlas Press: Beijing, China (in Chinese).
434 Chen, Z.Y, Stanley, D. J., 1995. Quaternary subsidence and river channel migration in the Yangtze
435 delta plain, eastern China. Journal of Coastal Research. 11, 927-945.
436 Chen, J., Wang, Z.H., Chen, Z.Y., Wei, Z.X., Wei, T.Y., Wei, W., 2009. Diagnostic heavy minerals
437 in Plio-Pleistocene sediments of the Yangtze Coast, China with special reference to the Yangtze
438 River connection into the sea. Geomorphology. 113, 129-136.
439 Chmeleff, J., Blanckenburg, F., Kossert, K., Jakob, D., 2010. Determination of the ^{10}Be half-life by
440 multi collector ICP-MS and liquid scintillation counting. Nuclear Instruments and Methods in
441 Physics Research Section B. 268, 192-199.
442 Chung, S.L., Lo, C.H., Lee, T.Y., Zhang, Y.Q., Xie, Y.W., Li, X.H, Wang, K.L., Wang, P.L., 1998.
443 Diachronous uplift of the Tibetan plateau starting 40 Myr ago. Nature. 394, 769-773.

444 Clark, M.K., Schoenbohm, L.M., Royden, L.H., Whipple, K.X., Burchfiel, B.C., Zhang, X., Tang,
445 W., Wang, E., Chen, L., 2004. Surface uplift, tectonics, and erosion of eastern Tibet from large-
446 scale drainage patterns. Tectonics. 23, 1-20.
447 Clift, P.D., Long, H.V., Hinton, R., Ellam, R.M., Hannigan, R., Tan, M.T., Blusztajn, J., Duc, N.A.,
448 2008. Evolving east Asian river systems reconstructed by trace element and Pb and Nd isotope
449 variations in modern and ancient Red River-Song Hong sediments. Geochemistry, Geophysics,
450 Geosystems. 9, Q04039.
451 Fan, D., Li, C., Yokoyama, K., Zhou, B., Li, B., Wang, Q., Yang, S., Deng, B., Wu, G., 2005.
452 Monazite age spectra in the Late Cenozoic strata of the Changjiang delta and its implication on
453 the Changjiang run-through time. Science China Ser. D. 48, 1718-1727.
454 Fu, X.W., Zhu, W.L., Geng, J.H., Yang, S.Y., Zhong, K., Huang, X.T., Zhang, L.Y., Xu, X., 2021.
455 The present-day Yangtze River was established in the late Miocene: Evidence from detrital
456 zircon ages. Journal of Asian Earth Sciences. 205, 104600.
457 Granger, D.E., Muzikar, P.F., 2001. Dating sediment burial with in situ-produced cosmogenic
458 nuclides: theory, techniques, and limitations. Earth and Planetary Science Letters. 188, 269-281.
459 Granger, D.E., 2006. A review of burial dating methods using ^{26}Al and ^{10}Be. Geological Society of
460 America Special Papers. 415, 1-16.
461 Granger, D.E., 2014. Cosmogenic nuclide burial dating in archaeology and paleoanthropology. In:
462 Turekian, K. and Holland, H. (Eds.), Treatise on Geochemistry, second ed., vol. 14, pp. 81-97.
463 Elsevier Publishing.
464 Gu, J.W., Chen, J., Sun, Q.L., Wang, Z.H., Wei, Z.X., Chen, Z.Y., 2014. China's Yangtze delta:
465 geochemical fingerprints reflecting river connection to the sea. Geomorphology. 227, 166-173.

466 Heisinger, B., Lal, D., Jull, A., Kubik, P., Ivy-Ochs, S., Neumaier, S., Knie, K., Lazarev, V.,
467 Nolte, E., 2002a. Production of selected cosmogenic radionuclides by muons: 1. Fast muons.
468 Earth Planetary Science Letters. 200, 345-355.
469 Heisinger, B., Lal, D., Jull, A., Kubik, P., Ivy-Ochs, S., Knie, K., Nolte, E., 2002b. Production
470 of selected cosmogenic radionuclides by muons: 2. Capture of negative muons. Earth Planetary
471 Science Letters. 200, 357-369.
472 Huang, X.T., Zheng, H.B., Yang, S.Y., Xie, X., 2009. Investigation of sedimentary geochemistry of
473 core DY03 in the Yangtze delta: Implications to tracing provenance. Quaternary Sciences. 29,
474 299-307. (In Chinese)
475 Jia, J.T., Zheng, H.B., Huang, X.T., Wu, F.Y., Yang, S.Y., Wang, K., He, M.Y., 2010. Detrital zircon
476 U-Pb ages of Late Cenozoic sediments from the Yangtze delta: Implication for the evolution
477 of the Yangtze River. Chinese Science Bulletin. 55, 1520-1528.
478 Jin, X., Yu, P., 1982. Geology of the Yellow Sea and the East China Sea. Science Press: Beijing,
479 pp.1-22. (in Chinese)
480 Kohl, C.P., Nishiizumi, K., 1992. Chemical isolation of quartz for measurement of in-situ-produced
481 cosmogenic nuclides. Geochemica et Cosmochimica Acta. 56, 3583-3587.
482 Kong, P., Zheng, Y., Caffee, M.W., 2012. Provenance and time constrain on the formation of the
483 first bend of the Yangtze River. Geochem. Geophys. Geosyst. 13, Q06017.
484 Li, J.J., Xie, S.Y., Kuang, M.S., 2001. Geomorphic evolution of the Yangtze Gorges and the time of
485 their formation. Geomorphology. 41, 125-135.
486 Li, B., Wei, Z., Li, X., He, Z., Zhang, K., Wang, Z., 2011. Records from quaternary sediment and
487 palaeo-environment in the Yangtze River delta. Quaternary Science. 31, 316-325. (in Chinese)

488 Liu, Y., Wang, S.J., Xu, S., Fabel, D., Liu, X.M., Zhang, X.B., Luo, W.J., Cheng, A.Y., 2013. New
489 evidence for the incision history of the Liuchong River, Southwest China, from cosmogenic
490 $^{26}Al/^{10}Be$ burial ages in cave sediments. Journal of Asian Earth Sciences. 73, 274-283.
491 Liu, J., Shi, X., Liu, Q., Ge, S., Liu, Y., Yao, Z., Zhao, Q., Jin, C., Jiang, Z., Liu, S., Qiao, S., Li, X.,
492 Li, C., Wang, C., 2014. Magnetostratigraphy of a greigite-bearing core from the south Yellow
493 Sea: implications for re-magnetization and sedimentation. Journal of Geophysical Research.
494 119, 7425-7441.
495 Liu, X.B., 2018. The study of magnetic properties of Late Cenozoic sediments on south and north
496 flanks of Yangtze delta: source-sink implications for river's connection to the sea. PH.D Thesis,
497 East China Normal University. (in Chinese with English abstract).
498 Liu, X.B., Chen, J., Maher, B.A., Zhao, B.C., Yue, W., Sun, Q.L., Chen, Z.Y., 2018. Connection of
499 the proto-Yangtze River to the East China Sea traced by sediment magnetic properties.
500 Geomorphology. 303, 162-171.
501 Masarik, J., Reedy, R.C., 1995. Terrestrial cosmogenic nuclide production systematic calculated
502 from numerical simulations. Earth and Planetary Science Letters. 136, 381- 395.
503 McPhillips, D., Hoke, G.D., Zeng-Liu, J., Bierman, P.R., Rood, D.H., Niedermann, S., 2016. Dating
504 the incision of the Yangtze River gorge at the First Bend using three-nuclide burial ages.
505 Geophysical Research Letters. 43, 101-110.
506 Mei, X., Li, R., Zhang, X., Liu, Q., Liu, J., Wang, Z., Lan, X., Liu, J., Sun, R., 2016. Evolution of
507 the Yellow Sea warm current and the Yellow Sea cold water mass since the middle Pleistocene.
508 Palaeogeogr. Palaeoclimatol. Palaeoecol. 442, 48-60.
509 Molnar, P., Tapponnier, P., 1975. Cenozoic tectonics of Asia: Effects of continental collision.

510 Science. 189, 419-426.
511 Molnar, P., England, P. and Martinod, J., 1993. Mantle dynamics, the uplift of the Tibetan Plateau
512 and the Indian monsoon. Reviews of Geophysics. 31, 357-396.
513 Morton, A.C., 1984. Stability of detrital heavy tertiary sandstones from sea basin minerals in the
514 North Sea Basin. Clay Minerals. 19, 287-308.
515 Nishiizumi, K., 2004. Preparation of ^{26}Al AMS standards. Nuclear Instruments and Methods in
516 Physics Research Section B. 223, 388-392.
517 Qiang, J., Weifeng, W., Huaimin, X., Shaochun, Y., Ji, Q., 1997. North Jiangsu Basin, eastern China:
518 accumulation of immature oils and diagenesis of Paleogene reservoir rocks. Journal of
519 Petroleum Geology. 20, 287-306.
520 Qin, Y., Zhao, Y., Chen, L., Zhao, S., 1989. Geology of the Yellow Sea. Oceanic Publish House,
521 Beijing, pp. 1-289 (in Chinese).
522 Ren, J.Y., Tamaki, K., Li, S.T., Zhang, J.X., 2002. Late Mesozoic and Cenozoic rifting and its
523 dynamic setting in Eastern China and adjacent areas. Tectonophysics. 344, 175-205.
524 Richardson, N.J., Densmore, A.L., Seward, D., Fowler, A., Wipf, M., Ellis, M.A., Li, Y., Zhang, Y.,
525 2008. Extraordinary denudation in the Sichuan Basin: Insights from low-temperature
526 thermochronology adjacent to the eastern margin of the Tibetan Plateau. Journal of Geophysical
527 Research. 113, B04409.
528 Richardson, N.J., Densmore, A.L., Seward, D., Wipf, M., Li, Y., 2010. Did incision of the Three
529 Gorges begin in the Eocene? Geology. 38, 551-554.
530 Saito, Y., Yang, Z.S., Hori, K., 2001. The Huanghe (Yellow River) and Changjiang (Yangtze River)
531 deltas: a review on their characteristics, evolution and sediment discharge during the Holocene.

Geomorphology. 41, 219-231.

Shao, L., Li, C.A., Yuan, S.Y., Kang, C.G., Wang, J.T., Li, T., 2012. Neodymium isotopic variations of the late Cenozoic sediments in the Jianghan Basin: Implications for sediment source and evolution of the Yangtze River. Journal of Asian Earth Sciences. 45, 57-64.

Shao, L., Yuan, S.Y., Li, C.A., Kang, C.G., Zhu, W.J., Liu, Y.D., Wang J.T., 2015. Changing provenance of late Cenozoic sediments in the Jianghan Basin. Geoscience Frontiers. 6, 605-615.

Sun, X.L., Tian, Y.T., Kuiper, K.F., Li, C.A., Zhang, Z.J., Wijbrans, J.R., 2021. No Yangtze River prior to the late Miocene: evidence from detrital muscovite and K-feldspar $^{40}Ar/^{39}Ar$ geochronology. Geophysical Research Letters. 10.1029/2020GL089903.

Tapponnier, P., Xu, Z.Q., Roger, F., Meyer, B., Arnaud, N., Wittlinger, G., Yang, J.S., 2001. Oblique stepwise rise and growth of the Tibet Plateau. Science. 294, 1671-1677.

Wageman, J.M., Hilde, T.W., Emery, K., 1970. Structural framework of east China sea and Yellow Sea. American Association of Petroleum Geologists Bulletin. 54, 1611-1643.

Wang, C.S., Zhao, X.X., Liu, Z.F., Lippert, P.C., Graham, S.A., Coe, R.S., Yi, H.S., Zhu, L.D., Liu, S., Li, Y.L., 2008. Constraints on the early uplift history of the Tibetan Plateau. PNAS. 105, 4987-4992.

Wang, P.X., 2004. Cenozoic deformation and the history of sea land interactions in Asia, in Continent-Ocean Interactions in the East Asian Marginal Seas. Geophys. Monogr. Ser., vol. 149, edited by P. Clift et al., pp. 1-22, AGU, Washington, D. C.

Wang, P., Zheng, H.B., Chen, L., Chen, J., Xu, Y., Wei, X., Yao, X., 2014. Exhumation of the Huangling anticline in the Three Gorges region: Cenozoic sedimentary record from the western

554 Jianghan Basin, China. Basin Research. 26, 505-522.

555 Wang, Z., Yang, S., Li, P., Li, C., Cai, J., 2006. Detrital mineral compositions of the Changjiang
556 River sediments and their tracing implications. Acta Sedimentologica Sinica. 24, 570-578.

557 Xiang, F., Zhu, L.D., Wang, C.S., Zhao, X.X., Chen, H.D., Yang, W.G., 2007. Quaternary sediment
558 in the Yichang area: Implications for the formation of the Three Gorges of the Yangtze River.
559 Geomorphology. 85, 249-258.

560 Xu, S., Freeman, S., Rood, D.H., Shanks, R.P., 2015. Decadal ^{10}Be, ^{26}Al and ^{36}Cl QA measurements
561 on the SUERC 5 MV accelerator mass spectrometer. Nuclear Instruments and Methods in
562 Physics Research B. 361, 39-42.

563 Yang, S., Li, C., Yokoyama, K., 2006. Elemental compositions and monazite age patterns of core
564 sediments in the Changjiang Delta: implications for sediment provenance and development
565 history of the Changjiang River. Earth Planetary Science Letter. 245, 762-776.

566 Yi, L., Ye, X., Chen, J., Li, Y., Long, H., Wang, X., Du, J., Zhao, S., Deng, C., 2014.
567 Magnetostratigraphy and luminescence dating on a sedimentary sequence from northern East
568 China Sea: constraints on evolutionary history of eastern marginal seas of China since the Early
569 Pleistocene. Quaternary International. 349, 316-326.

570 Yi, L., Deng, C., Tian, L., Xu, X., Jiang, X., Qiang, X., Qin, H., Ge, J., Chen, G., Su, Q., 2016. Plio-
571 Pleistocene evolution of Bohai basin (East Asia): demise of Bohai paleolake and transition to
572 marine environment. Science Report. 6, 29403.

573 Yu, J.J., Yue, W., Liu, P., Peng, B., Zhang, J., Sun, D.D., Wang, J.L., Lv, H.L., Chen, J., 2020.
574 Provenance Shift during the Plio-Pleistocene in the Vertex of Yangtze Delta and Its
575 Geomorphological Implications. Minerals. DOI: 10.3390/min10110996.

576 Yue, W., Liu, J.T., Zhang, D., Wang, Z.H., Zhao, B.C., Chen, Z.Y., Chen. J., 2016. Magnetite with
577 anomalously high Cr_2O_3 as a fingerprint to trace upper Yangtze sediments to the sea.
578 Geomorphology. 268, 14-20.
579 Yue, W., Yang, S., Zhao, B., Chen, Z., Yu, J., Liu, X., Huang, X., Jin, B., Chen, J., 2019. Changes
580 in environment and provenance within the Changjiang (Yangtze River) Delta during Pliocene
581 to Pleistocene transition. Marine Geology. 416, 105976.
582 Zhang, Y.F., Li, C.A., Wang, Q.L., Chen, L., Ma, Y.F., Kang, C.G., 2008. Magnetism parameters
583 characteristics of drilling deposits in Jianghan Plain and indication for forming of the Yangtze
584 River Three Gorges. Chinese Science Bulletin. 53, 584-590.
585 Zhang, J., Wan, S.M., Clift, P.D., Huang, J., Yu, Z.J., Zhang, K.D., Mei, X., Liu, J., Han, Z.Y., Nan,
586 Q.Y., Zhao, D.B., Li, A.C., Chen, L.H., Zheng, H.B., Yang, S.Y., Li, T.G., Zhang, X.H., 2019.
587 History of Yellow River and Yangtze River delivering sediment to the Yellow Sea since 3.5 Ma:
588 Tectonic or climate forcing? Quaternary Science Reviews. 216, 74-88.
589 Zheng, H.B., Clift, P.D., Wang, P., Tada, R., Jia, J.T., He, M.Y., Jourdan, F., 2013. Pre-Miocene birth
590 of the Yangtze River. PNAS. 110, 7556-7561.